RSC Advances

PAPER

View Article Online
View Journal | View Issue

Cite this: *RSC Adv.*, 2025, **15**, 13763

Uric acid detection *via* dual-mode mechanism with copper-coordinated nitrogen-doped carbon dots as peroxidase mimics†

Yousef A. Bin Jardan,[a] Mohamed M. El-Wekil, *[b] Mohamed R. Elmasry[c] and Al-Montaser Bellah H. Ali[b]

Monitoring disease-related biomarkers, such as uric acid in human body fluids, is essential for effective disease management and clinical diagnosis. In this study, copper-coordinated nitrogen-doped carbon dots (Cu@N-CDs) were synthesized *via* a simple hydrothermal method, achieving a remarkable photoluminescence quantum yield of 44.69%. The Cu@N-CDs emitted fluorescence at 460 nm upon excitation at 360 nm, making them highly suitable for sensitive biosensing applications. For uric acid detection, a Cu@N-CDs-based probe was developed and coupled with phenol (ph-OH) and 4-aminoantipyrine (AP-NH_2). In the presence of hydrogen peroxide (H_2O_2), generated through the enzymatic breakdown of uric acid by uricase, ph-OH and AP-NH_2 reacted to form a pink-colored compound. This compound quenched the fluorescence emission of Cu@N-CDs *via* an inner-filter effect, enabling fluorometric detection. Additionally, for colorimetric detection, the pink compound was quantified by measuring absorbance at 510 nm. The detection strategy utilized the peroxidase-mimetic activity of Cu@N-CDs, which was further enhanced by the presence of Cu. Under optimized conditions, the fluorometric method demonstrated a linear detection range of 0.01–700 μM, while the colorimetric method showed a range of 0.07–700 μM for uric acid. The developed approach proved highly effective in detecting uric acid in human blood serum and urine samples, yielding accurate results with acceptable recovery rates. This dual-mode detection method offers a reliable, sensitive, and cost-effective tool for monitoring uric acid levels, marking a significant advancement in clinical diagnostics and personalized healthcare.

Received 12th March 2025
Accepted 15th April 2025

DOI: 10.1039/d5ra01797a

rsc.li/rsc-advances

1. Introduction

Uric acid is a significant biomarker found in both urine and blood, playing a critical role in monitoring metabolic and renal health.[1] It is a by-product of purine metabolism, which occurs primarily in the liver, where purine bases are broken down to produce uric acid.[2] The levels of uric acid in the human body vary depending on factors such as sex, age, diet, and kidney function. Normal uric acid levels range from 0.088 to 0.455 mmol L^{-1} in women and 0.149 to 0.416 mmol L^{-1} in men.[3] When uric acid levels exceed 0.420 mmol L^{-1}, a condition called hyperuricemia may develop, which is associated with various health complications.[4] Low levels of uric acid in blood and urine may indicate underlying metabolic disorders or contribute to conditions such as hepatitis or nephritis.[5] Conversely, elevated uric acid levels in blood or urine can result in the formation of uric acid crystals. These crystals often accumulate in joints, leading to a painful condition known as gout.[6,7] Chronic hyperuricemia is strongly associated with an elevated risk of cardiovascular diseases, including hypertension and atherosclerosis, as well as renal complications such as nephropathy and kidney stones. These health risks underscore the importance of regular monitoring of uric acid levels. Early detection facilitates timely interventions, enabling better management of metabolic, hepatic, and renal disorders, and reducing the likelihood of long-term complications. Monitoring also supports personalized treatment strategies, dietary adjustments, and lifestyle modifications to mitigate the adverse effects of abnormal uric acid levels. Uric acid has been previously quantified using various analytical techniques, including bi-enzyme colorimetry,[8] chemiluminescence,[9] UV/vis spectrometry,[10] and High-Performance Liquid Chromatography (HPLC) with electrochemical detection.[11] These methods provide high sensitivity and selectivity but often involve lengthy procedures, high costs, and complex instrumentation. These

[a]*Department of Pharmaceutics, College of Pharmacy, King Saud University, Riyadh, Saudi Arabia*

[b]*Department of Pharmaceutical Analytical Chemistry, Faculty of Pharmacy, Assiut University, Assiut, 71526, Egypt. E-mail: mohamed.elwakeel@pharm.aun.edu.eg; mohamed.mohamoud@ymail.com*

[c]*School of Chemical Engineering, Sungkyunkwan University (SKKU), Suwon, 16419, Republic of Korea*

† Electronic supplementary information (ESI) available. See DOI: https://doi.org/10.1039/d5ra01797a

limitations highlight the necessity for developing simpler, cost-effective, and efficient alternatives for uric acid detection. Fluorescence-based sensors provide several advantages, including simplicity, high sensitivity, rapid response times, and excellent selectivity. These attributes make fluorescence an accessible and effective technique for the detection and quantification of biomolecules. Additionally, the ability to operate under mild conditions and detect low concentrations further enhances the suitability of fluorescence-based sensors for various biological and clinical applications.[12–14]

Carbon dots (CDs), a novel class of nanoscale fluorescent materials, have recently attracted significant attention owing to their numerous benefits, including straightforward synthesis, versatile surface modification capabilities, tunable structures, and excellent performance in applications such as catalysis and sensing.[15–18] They typically have particle sizes ranging from 1 to 10.5 nm.[19] These nanoscale materials offer the ability to replicate the functions of natural enzymes, sharing comparable characteristics such as surface charge, shape, and size. Unlike natural enzymes, which are hindered by issues such as limited stability, high cost, and challenging storage requirements, CDs effectively address these limitations.[20] Doping with heteroatoms and surface functionalization are effective strategies for modifying the fluorescence properties of CDs. These modifications influence their electronic structures, particularly the energy band gap, enhancing their suitability for various analytical applications.[21–24] Metallic heteroatoms, particularly transition metals, possess additional electrons and unoccupied orbitals, facilitating the modification of electronic properties on the surface of CDs.[25–27] Moreover, metal ions can interact with CDs through complexation chemical reactions, further enhancing their functional properties.[28] Copper (Cu), a more cost-effective and accessible alternative to gold (Au), has been demonstrated to enhance the photochemical performance of CDs, including improved electron transfer and chemical reactivity capabilities.[29] Additionally, unsaturated copper species (Cu^0 and Cu^+) are anticipated to exhibit reductive properties, enabling them to scavenge hydroxyl radicals (˙OH) during Fenton reactions.[30]

Building on these findings, a straightforward, reliable, and selective dual-mode sensor was developed for the detection of uric acid, incorporating both colorimetric and fluorometric capabilities. The probe utilized Cu@N-CDs, which exhibit peroxidase-like activity. In the presence of Cu@N-CDs, the enzymatic hydrolysis of uric acid by uricase produced H_2O_2, facilitating the coupling reaction between ph-OH and AP-NH_2. This reaction resulted in the formation of a pink-to-red chromogen with a strong absorbance peak at 510 nm. Concurrently, the fluorescence emission of Cu@N-CDs was quenched due to the presence of the colored chromogen, enabling dual-mode detection. The proposed sensor offers several advantages over conventional detection systems, including a broad dynamic linear range, high selectivity, ease of synthesis, and enhanced reliability. Notably, this dual-mode approach allows the detection of uric acid using two distinct techniques—colorimetry and fluorometry—by measuring signals at separate wavelengths. This capability provides greater analytical versatility and accuracy compared to traditional methods that typically rely on a single wavelength and detection mechanism. This innovative approach not only improves the sensitivity and reliability of uric acid detection but also demonstrates potential for broader applications in biomarker monitoring and clinical diagnostics.

2. Experimental

2.1. Materials and reagents

Uric acid (99.8%), uricase enzyme, ascorbic acid (AA, 98.7%), cysteine (Cys, 99.3%), glutathione (GSH, 98.4%), creatinine (CRE, 96.5%), glucose (Glu, 98.7%), dopamine (DA, 98.4%), quinine sulfate (98.8%), 3,3′,5,5′-tetramethylbenzidine (TMB, 98.7%), 4-aminoantipyrine (AP-NH_2), and phenol (ph-OH, AR) were sourced from Sigma Aldrich. Copper chloride dihydrate ($CuCl_2 \cdot 2H_2O$), sodium dihydrogen phosphate, ethylenediamine, disodium hydrogen phosphate, sodium hydroxide, and hydrochloric acid were obtained from Merck. All chemicals and reagents used in this experiment were of analytical grade.

2.2. Instrumentation and quantum yield

All the relevant details regarding the instrumentation used and the calculation of the quantum yield are thoroughly described in the ESI.†

2.3. Preparation of Cu@N-CDs

A simple hydrothermal process was used to prepare Cu@N-CDs as follows: 1.08 g of $CuCl_2 \cdot 2H_2O$ was mixed with 1.28 mL of ethylenediamine and 30 mL of ultrapure water. The mixture was then sonicated for 5 minutes and autoclaved at 200 °C for ten hours. After cooling, the yellow-colored product was collected by centrifugation at 5000 rpm and filtered using a 0.22 μm filter paper. The resulting product was dialyzed in dialysis bags (MWCO = 3 kDa) against pure water for 24 hours. Finally, the filtrate was freeze-dried to obtain the CDs powder. For comparison, N-CDs and pristine CDs were prepared following the same procedure, using ethylenediamine and glucose as precursors, respectively.

2.4. Detection of uric acid

The detection involved a hydrolysis step using the uricase enzyme to generate H_2O_2, followed by determination using Cu@N-CDs. The hydrolysis process was conducted as follows: 350 μL of various concentrations of uric acid were mixed with 50 μL of 2.5 mg per mL uricase enzyme and 100 μL of phosphate buffer (pH 8.5), then incubated at 37 °C for 20 minutes. For the detection step, 300 μL of 15.0 mM ph-OH, 300 μL of 15.0 mM AP-NH_2, 600 μL of phosphate buffer (pH 3.5), and 300 μL of 5.0 mg per mL Cu@N-CDs were added to the hydrolyzed solution (uric acid/uricase). The mixture was incubated at 55 °C for 25 minutes. Fluorescence emissions were recorded at 460 nm with an excitation wavelength of 360 nm, and colorimetric determination was performed at the maximum wavelength of 510 nm.

2.5. Steady-state kinetic assays

To study the kinetics of Cu@N-CDs, the material was tested with varying concentrations of H_2O_2 and TMB, and the time-dependent absorbance changes were recorded. H_2O_2 concentrations were varied in the range of 0.1–2.2 mM, while the TMB concentration was kept constant at 12 mM. Conversely, the H_2O_2 concentration was fixed at 0.8 mM, and the TMB concentration was varied from 2 to 26 mM. In all experiments, the absorbance of the blue-colored reaction product was measured at 654 nm. The kinetic parameters K_m (Michaelis constant) and V_m (maximum reaction velocity) were determined using the Michaelis–Menten equation (eqn (1)) and the Lineweaver–Burk equation (eqn (2)). In these equations, V represents the initial reaction velocity, and $[S]$ is the substrate concentration.

$$V = V_{max} \times [S]/(K_m + [S]) \quad (1)$$

$$1/V = (K_m/V_{max})(1/[S]) + (1/V_{max}) \quad (2)$$

2.6. Preparation of samples

Blood plasma was collected from healthy, non-smoking volunteers at Assiut University Hospital with informed consent. For serum preparation, 0.5 mL plasma was mixed with 0.75 mL acetonitrile and centrifuged at 4000 rpm for 20 minutes. The supernatant was stored at 4 °C for analysis. Urine samples (1.0 mL) were similarly centrifuged and filtered using medium-grade paper to remove particulates.

2.7. Ethical approval

Ethical approval was obtained from the Institutional Ethics Committee, University of Assiut. Written informed consent was secured from all participants before sample collection. All procedures complied with applicable regulations for the use of human specimens in biomedical research. Participant privacy and safety were maintained during collection, handling, analysis, and disposal of samples.

3. Results and discussions

3.1. Characterization

The morphological characteristics of Cu@N-CDs were analyzed using Transmission Electron Microscopy (TEM), revealing a spherical shape with an average size of 3.2 nm (Fig. S1A and B†). The HRTEM inset in Fig. S1A† shows lattice fringes of 0.23 nm, corresponding to the [100] facet of sp^2-graphitic carbon.[31] The FT-IR spectra of N-CQDs and Cu@N-CDs (Fig. S1C†) display characteristic bands at: 3290 cm^{-1}: ν(OH), 3180 cm^{-1}: ν(NH), 2860 cm^{-1}: $\nu(CH_2)$,1695 cm^{-1}: ν(C=O), 1620 cm^{-1}: δ(OH), and 560 cm^{-1}: δ(NH).[32,33] Additionally, a new band at 690 cm^{-1}, attributed to ν(Fe–O), confirms the successful incorporation of Fe during Cu@N-CD fabrication. The Raman spectra (Fig. S1D†) exhibit two prominent bands: 1390 cm^{-1} (D-band): associated with disordered carbon, 1595 cm^{-1} (G-band): related to graphitic carbon. The D/G intensity ratios were 0.90 and 1.25 for N-CDs and Cu@N-CDs, respectively, indicating a higher degree of disordered carbon in Cu@N-CDs.[34] Fig. 1A presents the EDX pattern of Cu@N-CDs, showing identifiable peaks for Cu, C, N, and O. The PXRD patterns of N-CDs and Cu@N-CDs are displayed in Fig. 1B. The N-CDs exhibit a broad peak at approximately 22.3°, corresponding to graphitic carbon,[35,36] while additional diffraction peaks are observed in Cu@N-CDs, attributed to Cu doping. Fig. S2† presents the XPS analysis of the as-prepared Cu@N-CDs. Fig. S2A† displays the full XPS survey spectrum of Cu@N-CDs, showing distinct and well-separated peaks for C 1s (287.8 eV), N 1s (398.4 eV), O 1s (533.3 eV), and Cu 2p (947.6 eV). Fig. S2B† highlights the deconvoluted spectrum of C 1s, with three peaks at 284.5 eV, 286.4 eV, and 287.6 eV, attributed to C=C, C–O/C–N, and C=O, respectively. Fig. S2C† illustrates the deconvoluted spectrum of N 1s, showing peaks at 398.8 eV, 399.2 eV, and 399.9 eV, corresponding to pyridinic N, pyrrolic N, and graphitic N, respectively. Fig. S2D† explores the deconvoluted spectrum of O 1s, with sharp peaks at 531.4 eV and 533.8 eV, associated with C=O and C–O, respectively. Fig. S2E† demonstrates the deconvoluted spectrum of Cu 2p, revealing five distinct peaks. Peaks at 932.6 eV and 934.8 eV correspond to Cu $2p_{3/2}$ of Cu(I) and Cu(II), while peaks at 951.8 eV and 953.7 eV correspond to Cu $2p_{1/2}$ of Cu(I) and Cu(II). A weak, broad peak at 943.4 eV is identified as the Cu $2p_{3/2}$ satellite peak.[37] Fig. 2 presents the absorption and fluorescence characterization of the as-prepared Cu@N-CDs. Fig. 2A shows the absorption spectrum with distinct absorption bands at 220 nm and 335 nm, attributed to

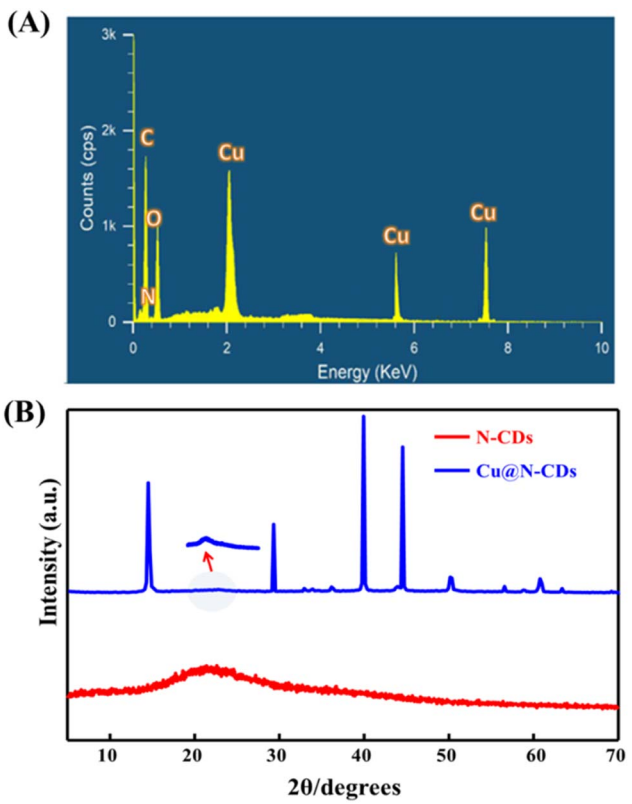

Fig. 1 EXD (A) and PXRD (B) patterns of Cu@N-CDs.

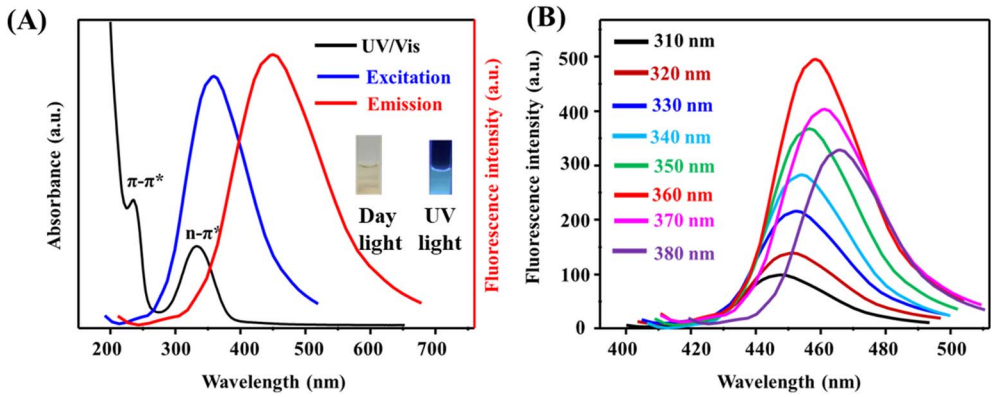

Fig. 2 (A) UV/vis and excitation/fluorescence spectra while (B) emission-dependent excitation of Cu@N-CDs.

π–π* and n–π* transitions, respectively. Additionally, the figure includes the excitation and emission spectra of Cu@N-CDs, observed at 360 nm and 460 nm, respectively. Fig. 2B demonstrates the dependency of emission wavelength and intensity on the excitation wavelength within the range of 310–380 nm. The results indicate that emission intensities increase and emission wavelengths exhibit a red shift with increasing excitation wavelength. This behavior suggests variations in the distribution of surface functional groups on the surface of Cu@N-CDs.[38,39] The stability of Cu@N-CDs probe was evaluated under various conditions, including different ionic strengths, different ion solutions (100 mM), pH values, irradiation times, and temperature values (Fig. S3†). The results demonstrate the probe's robustness across these conditions. Additionally, the quantum yield of the as-prepared CDs, N-CDsm and Cu@N-CDs were determined to be 33.78%, 37.65%, and 44.69%, respectively, calculated using quinine sulfate as the standard (refer to ESI† for details). The high quantum yield (44.69%) of the Cu@N-CDs is primarily attributed to the synergistic effects of nitrogen doping and copper coordination. Nitrogen atoms introduce surface functional groups such as pyridinic, pyrrolic, and graphitic nitrogen, which passivate surface defects and enhance electron delocalization, promoting radiative recombination. Simultaneously, copper ions (Cu^{+}/Cu^{2+}) coordinate with these nitrogen sites, modulating the electronic band structure and suppressing non-radiative pathways by minimizing trap states.[40] This coordination also enhances charge carrier separation and stabilizes excited states. Additionally, the well-defined graphitic core structure and uniform nanoscale size (~3.2 nm) contribute to efficient fluorescence emission. These combined structural and electronic features result in the remarkable photoluminescence efficiency observed in the Cu@N-CDs.

3.2. Quenching mechanism and peroxidase-mimetic activity of Cu@N-CDs

In the presence of H_2O_2, AP-NH_2 undergoes oxidative coupling with ph-OH to form a red-colored product exhibiting a maximum absorbance at 510 nm. The UV-vis absorption spectra for various systems, including Cu@N-CDs, Cu@N-CDs/H_2O_2, Cu@N-CDs/ph-OH, Cu@N-CDs/AP-NH_2, and Cu@N-CDs/H_2O_2/AP-NH_2/ph-OH, are presented in Fig. S4A.† Notably, a distinct absorption band at 510 nm was observed exclusively in the Cu@N-CDs/H_2O_2/AP-NH_2/ph-OH system, indicating the successful formation of the colored product. In contrast, systems lacking Cu@N-CDs exhibited no significant UV-vis absorption at 510 nm (Fig. S4B†), underscoring the critical role of Cu@N-CDs in catalyzing the reaction. To further investigate the individual contributions of Cu@N-CDs, AP-NH_2, ph-OH, and H_2O_2, a systematic survey of various combinations was conducted (Fig. S4C†). The results confirmed that the characteristic absorption band at 510 nm emerged only in the presence of Cu@N-CDs, H_2O_2, AP-NH_2, and ph-OH. It was clearly observed that only weak absorption bands appeared when CDs or N-CDs were used as substitutes for Cu@N-CDs. In contrast, a prominent absorption band was recorded exclusively with Cu@N-CDs, highlighting the critical role of copper doping in enhancing the catalytic efficiency of the platform (Fig. S4D†). It is important to note that doping CDs with copper (Cu) and nitrogen (N) significantly modulates their surface states and intrinsic electronic structures, leading to enhanced fluorescence emission properties (Fig. S4E†). This modification not only improves the optical characteristics of the CDs but also broadens their potential applications in catalytic and sensing systems. The quenching behavior of the red-colored product on the fluorescence emission of Cu@N-CDs was analyzed, as shown in Fig. S5A.† It was observed that only the system containing H_2O_2, AP-NH_2, and ph-OH (resulting in the red-colored product, quinoneimine) effectively quenched the fluorescence emission of Cu@N-CDs. In contrast, other systems exhibited negligible quenching effects, underscoring the specific interaction between the red-colored product and Cu@N-CDs. Furthermore, the absorption spectrum of the red-colored product was found to overlap with the emission spectrum of Cu@N-CDs, indicating the presence of an inner-filter effect between the two systems, Fig. S5B.†[41] To further validate this interaction, fluorescence lifetimes of Cu@N-CDs were measured both before and after the addition of the red-colored product. The results revealed that the fluorescence lifetimes were 4.67 ns for Cu@N-CDs and 4.65 ns for the Cu@N-CDs/

quinoneimine, demonstrating minimal variation (Fig. S5C†). This suggests that static quenching is the primary mechanism underlying the observed fluorescence suppression.[42,43]

3.3. Optimization of reaction variables

To improve detection sensitivity, various factors influencing the system's sensing performance were systematically evaluated (Fig. S6†). Fig. S6A† illustrates the effect of pH on the detection of uric acid. The results revealed that the catalytic performance of Cu@N-CDs was enhanced under acidic conditions, which promote the Fenton-like reaction facilitated by the incorporation of copper atoms into the CDs' framework.[44,45] Fig. S6B† illustrates the influence of hydrolysis temperature within the range of 40–65 °C on the fluorescence response. The optimum fluorescence response was observed at 55 °C, identified as the optimal temperature for uric acid hydrolysis. Beyond this temperature, a noticeable decline in fluorescence readings was recorded, likely due to the decomposition of H_2O_2 and the resultant red-colored product, which diminishes the system's overall stability and sensitivity. Fig. S6C† examines the effect of Cu@N-CDs concentration on the catalytic performance within the range of 3.0–6.5 mg mL^{-1}. The results indicated that the optimum fluorescence response was achieved at a Cu@N-CDs concentration of 5.0 mg mL^{-1}. Beyond this concentration, no significant change in fluorescence response was observed, suggesting a saturation point in the catalytic activity. Conversely, at concentrations below 5.0 mg mL^{-1}, the fluorescence response was notably reduced, likely due to insufficient Cu@N-CDs to effectively drive the catalytic reaction. Additionally, the effect of hydrolysis time on the catalytic performance was investigated over a range of 10–40 minutes (Fig. S6D†). The results showed that the optimum hydrolysis time was 25 minutes, which was subsequently adopted as the optimal value for further analyses. Finally, the effect of ph-OH and AP-NH_2 concentrations on the fluorescence response was evaluated (Fig. S6E and F†). The results indicated that the optimal concentrations for both compounds were 15.0 mM, yielding the highest fluorescence responses.

3.4. Dual-mode detection of uric acid

The colorimetric and fluorometric determination of uric acid using the uricase enzyme was enhanced by the peroxidase-like activity of fluorescent Cu@N-CDs (Scheme 1). In the colorimetric method, the red-colored product, exhibiting an absorption peak at 510 nm, was formed through the coupling oxidation reaction between AP-NH_2 and ph-OH in the presence of H_2O_2. The degradation of uric acid by the uricase enzyme generated H_2O_2, thereby increasing the red product's formation. This red-colored product quenched the fluorescence emission of Cu@N-CDs, enabling the fluorometric quantification of uric acid.

The colorimetric and fluorometric data for the quantification of uric acid are presented in Fig. 3. Fig. 3A shows the colorimetric absorption spectra, while Fig. 3B illustrates the corresponding calibration plot for uric acid determination, facilitated by enzymatic hydrolysis in the presence of AP-NH_2 and ph-OH. The results indicate that increasing uric acid concentrations led to a rise in absorbance values at 510 nm within the range of 0.07–700 μM. The linear regression equation describing the relationship between absorbance and uric acid concentration is given as: $A = 0.123 + 0.0014$[uric acid] with a determination coefficient (r^2) of 0.9907. The detection limit was calculated to be 0.02 μM. Fig. 3C illustrates the fluorescence spectra of Cu@N-CDs after the successive addition of uric acid concentrations (0.01–700 μM), facilitated by enzymatic hydrolysis in the presence of AP-NH_2 and ph-OH. The fluorescence emission of Cu@N-CDs was progressively quenched with increasing uric acid concentrations. Fig. 3D presents the calibration plot of fluorescence responses (F^0/F) *versus* uric acid concentration, with a regression equation of $F^0/F = 1.05 + 0.001$[uric acid] and a determination coefficient (R^2) of 0.9940. The detection limit was calculated to be 0.001 μM. Table 1 summarizes the analytical performance of the proposed system

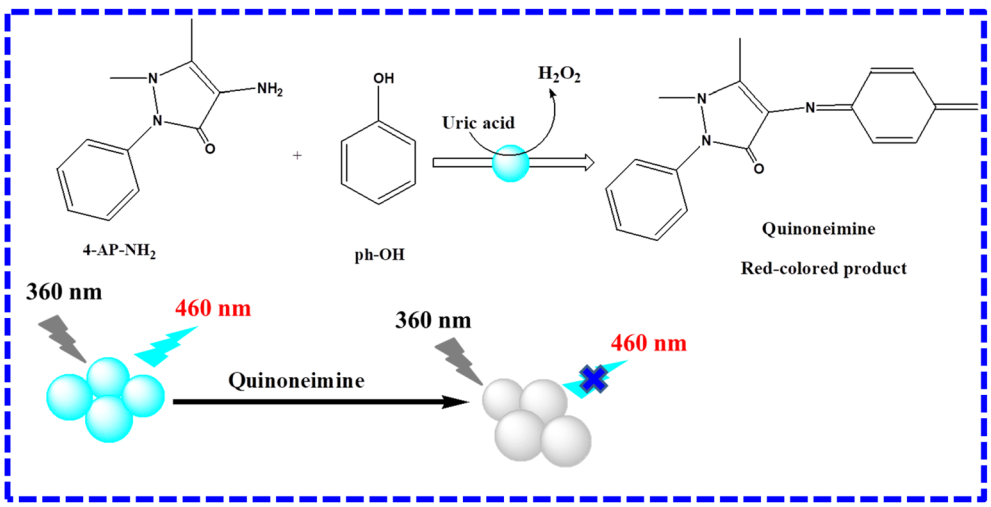

Scheme 1 Dual-mode detection of uric acid *via* Cu@N-CDs, AP-NH_2, uricase, and ph-OH.

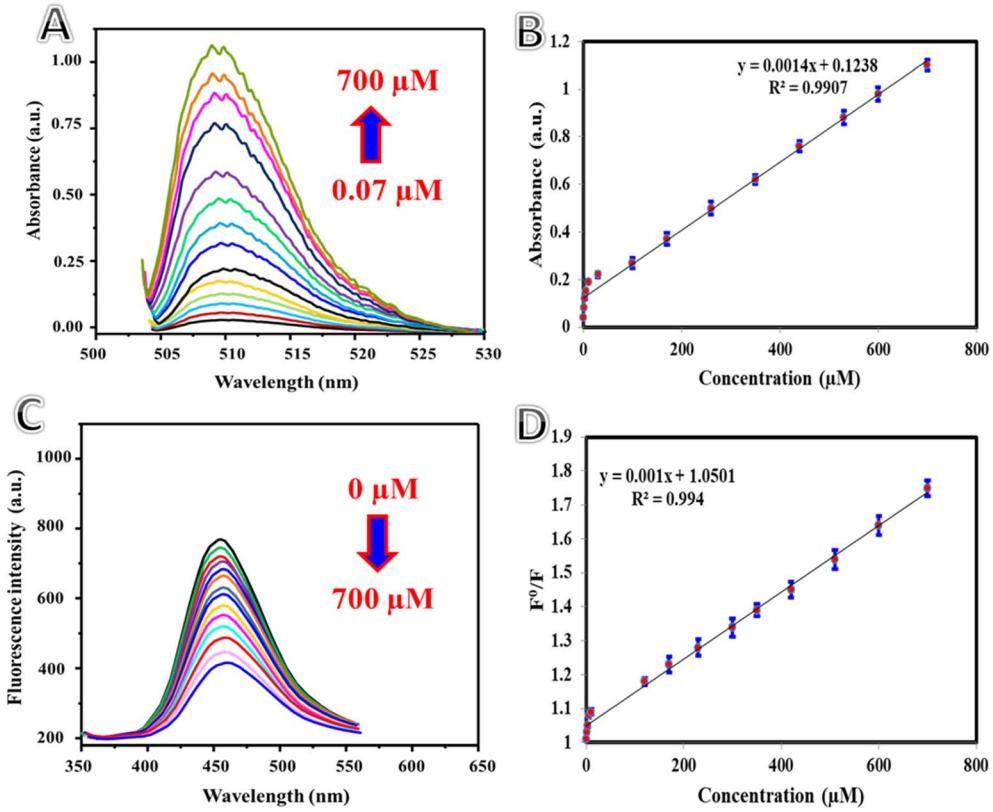

Fig. 3 (A) Absorption spectrum of AP-NH_2/ph-OH/uricase with Cu@N-CDs in the presence of varying concentrations of uric acid (0.07–700 µM); (B) calibration plot showing the relationship between absorbance values and uric acid concentration; (C) fluorescence spectra of AP-NH_2/ph-OH/uricase with Cu@N-CDs in the presence of varying concentrations of uric acid (0.01–700 µM); (D) calibration plot illustrating the relationship between fluorescence responses (F^0/F) and uric acid concentration.

for uric acid determination in comparison with other systems. The proposed system demonstrates notable advantages, including a wide linear range and a low detection limit, making it superior to existing methods. Furthermore, the reproducibility of the proposed methods was evaluated, as shown in Table 2. The results revealed that both the colorimetric and fluorometric methods exhibit a high degree of reproducibility, as evidenced by the low relative standard deviation (RSD) percentages.

3.5. Steady-state kinetics

The steady-state kinetics of the fabricated Cu@N-CDs were illustrated in Fig. S7A and B† by recording the absorbance at 654 nm. Additionally, the Lineweaver–Burk plots were

Table 1 Comparison between analytical parameters of the proposed dual-mode system and other colorimetric and fluorometric systems for detection of uric acid

System + uricase enzyme	Substrate	Linear range (µM)	LOD (µM)	Reaction time (minutes)	Reference
Colorimetric					
Fe_3O_4@MnO_2 NS	TMB	200–650	21	1	46
MoS_2/PDA/CoCu	TMB	0.5–200	0.13	40	47
Polypyrrole	TMB	200–1000	65	70	48
Cu@hydroxyapatite	TMB	1–270	0.24	100 (s)	49
Au@cellulose membrane	TMB	7–1400	7	18	50
N-CDs	OPD	0.5–150	0.06	30	51
Cu@N-CDs	AP-NH_2/ph-OH	0.07–700	0.02	25	This work
Fluorometric					
Papain	OPD	10–1000	4.6	15	52
Fe/N-CDs	OPD	0.5–100	0.14	30	53
BSA@Au NCs	TMB	0.50–50	0.39	60	54
Cu@N-CDs	AP-NH_2/ph-OH	0.01–700	0.001	25	This work

Table 2 Reproducibility of the colorimetric and fluorometric methods ($n = 5$)

Concentration (μM)	Colorimetric			Fluorometric		
	Found (μM)	Recovery %	RSD %	Found (μM)	Recovery %	RSD %
5.0	4.97	99.4	2.43	5.17	103.4	2.67
100.0	99.21	99.21	1.87	102.73	102.7	3.25
500.0	505.41	101.2	2.98	507.27	101.5	3.53

constructed and presented in Fig. S7C and D.† Table 3 provides a summary of the kinetic parameters of Cu@N-CDs, comparing them with horseradish peroxidase (HRP) and other peroxidase mimics. The data clearly show that Cu@N-CDs exhibit a high V_{max} and a low K_m, indicating their superior catalytic efficiency compared to HRP and other nanozymes. These findings highlight the potential of Cu@N-CDs for the effective determination of H_2O_2 and uric acid.

3.6. Stability, reproducibility, and reversibility

The stability of the synthesized Cu@N-CDs was evaluated over a period of 56 days. During this time, the relative activity (RA %) was monitored and found to decrease slightly by the end of the period. This decline suggests good long-term stability of the nanozyme. The observed reduction in RA % may be attributed to changes in the particle size of the catalyst over time. Furthermore, the reproducibility of the proposed sensor was assessed by preparing eight different batches under identical fabrication conditions. The relative standard deviation (RSD %) across the batches was found to be no more than 3.43%, demonstrating the sensor's reliability for detecting uric acid. Static quenching typically involves the formation of a non-fluorescent complex, which is generally not reversible, especially under the experimental conditions used in the study.

3.7. Anti-interference studies

The ability of an analytical method to selectively detect the target analyte is critical for its practical applications. To evaluate selectivity and anti-interference properties, various potential interfering species were tested, including 500 μM ions (Na^+, K^+, Ca^{2+}, Mg^{2+}, HCO_3^-) and 20 μM biomolecules (glucose, cysteine, epinephrine, dopamine, glutathione, and ascorbic acid) (Fig. 4). The results indicate that the colorimetric and fluorometric methods demonstrate good anti-interference capabilities for uric acid detection. This selectivity is likely due to the specific hydrolysis of uric acid catalyzed by the uricase enzyme. However, certain compounds, such as ascorbic acid, cysteine, dopamine, epinephrine, and glutathione, were found to interfere with the reaction. These interferences are attributed to the compounds' ability to reduce hydroxyl radicals ($OH^•$), which are crucial for catalyzing the oxidative coupling mechanism.[64,65] Since the concentrations of ascorbic acid, cysteine, dopamine, epinephrine, and glutathione in urine and serum are significantly lower than that of uric acid, their interference can be minimized by diluting the biological fluids.[66,67] Although Fe^{3+} can quench fluorescence in controlled environments, their low free-ion concentration, protein-bound state, and dilution during sample preparation make their quenching effect on Cu@N-CDs negligible in practical biological applications.

Table 3 Comparison of K_m and V_{max} between Cu@N-CDs and other nanozymes

Nanozyme	Substrate	K_m (mm)	V_{max} ($\times 10^{-7}$ M s^{-1})	Reference
Horseradish peroxidase	H_2O_2	3.70	8.71	55
	TMB	0.43	10.0	
Hemin-graphene	H_2O_2	2.74	3.53	56
	TMB	4.84	4.69	
Fe-MIM/ZIF-8	H_2O_2	0.02	8.05	57
	TMB	2.51	20.07	
Vanadium penta-oxide	H_2O_2	0.29	20.06	58
	TMB	0.69	27.15	
MIL-53(Fe)	H_2O_2	0.04	1.86	59
	TMB	1.08	8.78	
Fe-MIL-88-NH_2	H_2O_2	0.21	7.04	60
	TMB	0.28	10.47	
MoS_2@$MgFe_2O_4$	H_2O_2	0.24	3.78	61
	TMB	0.81	14.13	
2D Fe-CTF	H_2O_2	0.17	61.5	62
	TMB	0.04	66.2	
Au–Ag/L-Cys-rGO	H_2O_2	22.8	1.06	63
	TMB	0.27	0.82	
Cu@N-CDs	H_2O_2	0.12	57.34	This work
	TMB	0.08	52.87	

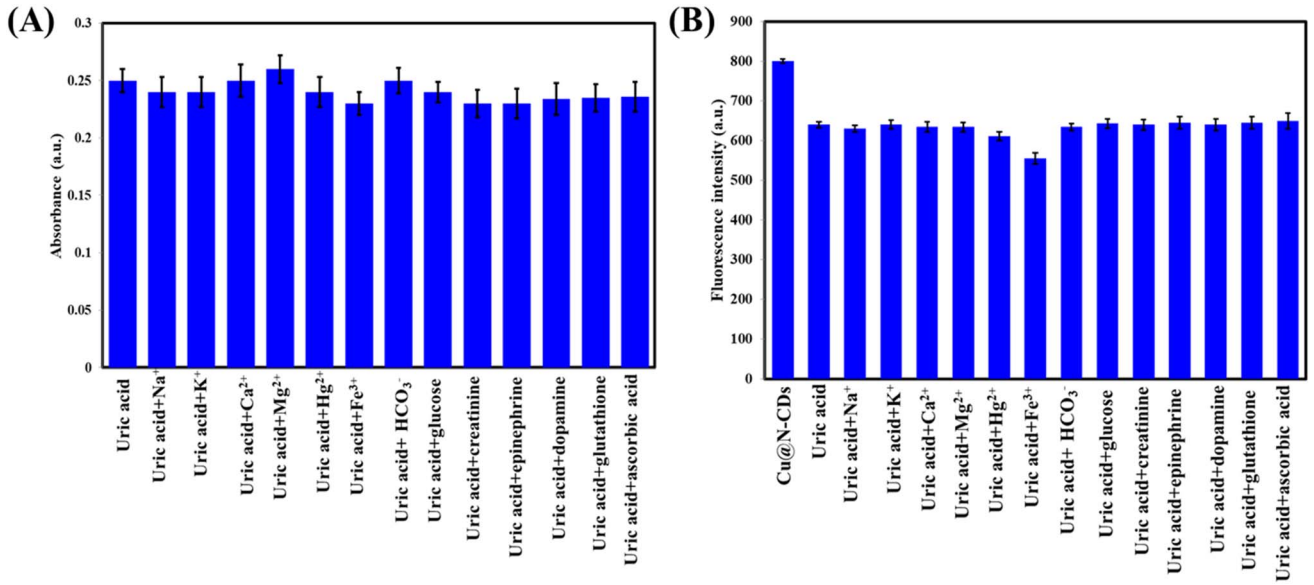

Fig. 4 Anti-interference studies were conducted on the Cu@N-CDs/AP-NH_2/ph-OH/uricase system for the determination of uric acid using the colorimetric method ((A) with a uric acid concentration of 30 μM) and the fluorometric method ((B) with a uric acid concentration of 120 μM). The concentrations of interfering ions and biomolecules were set at 500 μM and 20 μM, respectively.

Table 4 Detection of uric acid in human serum and urine samples using fluorometric method-based Cu@N-CDs/AP-NH_2/ph-OH/uricase system ($n = 3$)

Samples	Biochemistry analyzer	Proposed	Added	Found	Recovery %	RSD %
Serum 1	465 μM	474 μM	1.0 μM	470.7 μM	99.1	2.78
			5.0 μM	488.9 μM	102.1	3.23
			10.0 μM	488.1 μM	100.8	3.76
Serum 2	486 μM	468 μM	1.0 μM	463.8 μM	98.9	2.89
			5.0 μM	477.3 μM	100.9	3.65
			10.0 μM	485.4 μM	101.5	4.21
Urine 1	2.34 mM	—	1.0 mM	3.43 mM	102.7	2.67
			2.0 mM	4.43 mM	102.1	3.52
			3.0 mM	5.32 mM	99.6	3.20
Urine 2	2.23 mM	—	1.0 mM	3.35 mM	103.7	3.76
			2.0 mM	4.34 mM	102.6	3.29
			3.0 mM	5.28 mM	100.9	4.08

3.8. Real samples analysis

Serum and urine samples were analyzed using the Cu@N-CDs/AP-NH_2/ph-OH/uricase system (Table 4). The results from serum samples were compared with those obtained from a biochemistry analyzer. The recoveries were found to range from 98.9% to 103.7%, with RSDs between 2.67% and 4.21%. These results confirm the reliability and accuracy of the system for detecting uric acid in biological fluids.

4. Conclusions

This study successfully developed a dual-mode biosensor for uric acid detection based on copper- and nitrogen-doped carbon dots (Cu@N-CDs) synthesized *via* a hydrothermal method. The Cu@N-CDs exhibited a high photoluminescence quantum yield of 34.87%, enabling their application in both fluorometric and colorimetric detection modes. The probe, in combination with phenol (ph-OH), 4-aminoantipyrine (AP-NH_2), and hydrogen peroxide (H_2O_2) enzymatically generated by uricase, enabled sensitive detection of uric acid. Detection was achieved through fluorescence quenching of Cu@N-CDs at 460 nm and absorbance measurements of the pink-colored product at 510 nm. The fluorometric method demonstrated a detection range of 0.01–700 μM, while the colorimetric method exhibited a range of 0.07–700 μM. This dual-mode approach proved highly effective for analyzing uric acid in serum and urine samples, delivering high accuracy and recovery. It offers a cost-effective and reliable tool for clinical diagnostics and personalized healthcare applications.

Data availability

Data will be available upon request from the corresponding authors.

Conflicts of interest

The authors state that there are no conflicts of interest, financial or personal, that could have affected the integrity of this work.

Acknowledgements

The authors would like to extend their sincere appreciation to the Researchers Supporting Project, King Saud University, Riyadh, Saudi Arabia for funding this work through the project number (RSP2025R457).

References

1 A. Abellan-Llobregat, C. Gonzalez-Gaitan, L. Vidal, A. Canals and E. Morallon, Portable electrochemical sensor based on 4-aminobenzoic acid-functionalized herringbone carbon nanotubes for the determination of ascorbic acid and uric acid in human fluids, *Biosens. Bioelectron.*, 2018, **109**, 123–131.

2 G. Li, S. Liu, D. Liu and N. Zhang, MOF-derived porous nanostructured Ni_2P/C material with highly sensitive electrochemical sensor for uric acid, *Inorg. Chem. Commun.*, 2021, **130**, 108713.

3 J. S. Oh, S. W. Choi, B. S. Ku, S. C. Hong, Y. J. Kim, B. S. Koo, Y. G. Kim, C. K. Lee and B. Yoo, SAT0522 The association between uric acid level and urolithiasis on ultrasonography, *Ann. Rheum. Dis.*, 2014, **73**, 780.

4 C. Ben Salem, R. Slim, N. Fathallah and H. Hmouda, Drug-induced hyperuricaemia and gout, *Rheumatology*, 2017, **56**, 679–688.

5 C. Francesca, S. Pietro, M. C. Anna, M. Giovanni, A. Andrea, T. Luigi, C. Giacinto, G. Paola and M. C. Marco, Uric acid in metabolic and cerebrovascular disorders: a review, *Curr. Vasc. Pharmacol.*, 2020, **18**, 610–618.

6 B. Reeves, Significance of joint fluid uric acid levels in gout, *Ann. Rheum. Dis.*, 1965, **24**, 569.

7 M. H. Mahnashi, A. M. Mahmoud, M. M. El-Wekil and R. Y. Shahin, An innovative enzyme-free ratiometric determination of uric acid based on polyethyleneimine modified graphene quantum dots pretreated with periodate combined with eosin Y, *Microchem. J.*, 2023, **193**, 109062.

8 X. Chen, J. Chen, F. Wang, X. Xiang, M. Luo, X. Ji and Z. He, Determination of glucose and uric acid with bienzyme colorimetry on microfluidic paper-based analysis devices, *Biosens. Bioelectron.*, 2012, **35**, 363–368.

9 M. Saqib, L. Qi, P. Hui, A. Nsabimana, M. I. Halawa, W. Zhang and G. Xu, Development of luminol-N-hydroxyphthalimide chemiluminescence system for highly selective and sensitive detection of superoxide dismutase, uric acid and Co(2), *Biosens. Bioelectron.*, 2018, **99**, 519–524.

10 F. Olmo, J. Garoz-Ruiz, A. Colina and A. Heras, Derivative UV/Vis spectroelectrochemistry in a thin-layer regime: deconvolution and simultaneous quantification of ascorbic acid, dopamine and uric acid, *Anal. Bioanal. Chem.*, 2020, **412**, 6329–6339.

11 X. N. Li and A. A. Franke, Fast HPLC-ECD analysis of ascorbic acid, dehydroascorbic acid and uric acid, *J. Chromatogr. B*, 2009, **877**, 853–856.

12 A. M. Mahmoud, M. H. Mahnashi, A. Al Fatease, M. A. H. Mostafa, M. M. El-Wekil and R. Ali, Fluorometric and electrochemical dual-mode detection of toxic flavonoid rutin based on new nitrogen and sulfur co-doped carbon dots: Enhanced selectivity based on masking the interfering flavonoids with BSA complexation, *J. Food Compos. Anal.*, 2022, **108**, 104428.

13 S. A. Yahya, A. M. Mahmoud and M. M. El-Wekil, Ultrasensitive fluorometric determination of aluminum using the $CoFe_2O_4$ NPs/SDS/oxine system with the aid of ultrasound waves, *Anal. Methods*, 2024, **16**, 1804–1810.

14 B. A. Alyami, A. M. Mahmoud, A. O. Alqarni and M. M. El-Wekil, Intrinsic self-calibration electrostatic-controlled ratiometric fluorescence assay of histamine in human serum and canned tuna fish samples, *Microchem. J.*, 2023, **195**, 109388.

15 A. O. Alqarni, S. A. Alkahtani, A. M. Mahmoud and M. M. El-Wekil, Design of "Turn On" fluorometric nanoprobe based on nitrogen doped graphene quantum dots modified with β-cyclodextrin and vitamin B_6 cofactor for selective sensing of dopamine in human serum, *Spectrochim. Acta, Part A*, 2021, **248**, 119180.

16 K. Alhazzani, A. Z. Alanazi, A. M. Alaseem, S. A. Al Awadh, S. A. Alanazi, A. A. AlSayyari, M. M. Alanazi and M. M. El-Wekil, A reliable ratiometric fluorescence sensing of heparin and its antidote based on cationic carbon quantum dots and acid red 87, *Microchem. J.*, 2023, **190**, 108666.

17 R. M. K. Mohamed, S. H. Mohamed, A. M. Asran, I. H. Alsohaimi, H. M. A. Hassan, H. Ibrahim and M. M. El-Wekil, Bifunctional ratiometric sensor based on highly fluorescent nitrogen and sulfur biomass-derived carbon nanodots fabricated from manufactured dairy product as a precursor, *Spectrochim. Acta, Part A*, 2023, **293**, 122444.

18 H. R. H. Ali, A. I. Hassan, Y. F. Hassan and M. M. El-Wekil, Development of dual function polyamine-functionalized carbon dots derived from one step green synthesis for quantitation of Cu^{2+} and S^{2-} ions in complicated matrices with high selectivity, *Anal. Bioanal. Chem.*, 2020, **412**, 1353–1363.

19 H. R. H. Ali, A. I. Hassan, Y. F. Hassan and M. M. El-Wekil, Colorimetric and fluorometric nanoprobe for selective and sensitive recognition of hazardous colorant indigo carmine in beverages based on ion pairing with nitrogen doped carbon dots, *Food Chem.*, 2021, **349**, 129160.

20 S. N. Baker and G. A. Baker, Luminescent carbon nanodots: emergent nanolights, *Angew. Chem., Int. Ed.*, 2010, **49**, 6726–6744.

21 J. Tian, Q. Liu, A. M. Asiri, A. H. Qusti, A. O. Al-Youbi and X. Sun, Ultrathin graphitic carbon nitride nanosheets: a novel peroxidase mimetic, Fe doping-mediated catalytic performance enhancement and application to rapid, highly

sensitive optical detection of glucose, *Nanoscale*, 2013, **5**, 11604–11609.

22 Y. S. Park, J. H. Yoo, B. Lim, W. Kwon and S. W. Rhee, Improving the functionality of carbon nanodots: doping and surface functionalization, *J. Mater. Chem.*, 2016, **4**, 11582–11603.

23 J. Ge, Y. Yuan, H. Yang, R. Deng, Z. Li and Y. Yang, Smartphone-assisted colorimetric sensor based on single-atom Cu–C–N nanozyme for mercury (II) ions detection, *Mater. Today Chem.*, 2024, **37**, 102037.

24 J. Ge, L. Yang, Z. Li, Y. Wan, D. Mao, R. Deng, Q. Zhou, Y. Yang and W. Tan, A colorimetric smartphone-based platform for pesticides detection using Fe-N/C single-atom nanozyme as oxidase mimetics, *J. Hazard. Mater.*, 2022, **436**, 129199.

25 P. Zhu, Y. Liu, Y. Tang, S. Zhu, X. Liu, L. Yin, Q. Liu, Z. Yu, Q. Xu, D. Luo and J. Wang, Bi-doped carbon quantum dots functionalized liposomes with fluorescence visualization imaging for tumor diagnosis and treatment, *Chin. Chem. Lett.*, 2024, **35**, 108689.

26 Y. Liu, C. Guo, G. Wu, W. Lv, R. Zhou, W. Qiu, Y. Zhou, Q. Xu, C. Xu and Y. Niu, Uniformly dispersed bismuth metal nano catalyst modified carbon cloth electrode for iron-chromium flow battery, *Nano Res. Energy*, 2025, **4**, e9120135.

27 W. Liu, C. Li, Y. Ren, X. Sun, W. Pan, Y. Li, J. Wang and W. Wang, Carbon dots: surface engineering and applications, *J. Mater. Chem. B*, 2016, **4**, 5772–5788.

28 L. P. Lin, X. X. Luo, P. Y. Tsai, J. J. Wang and C. Xi, Metal ions doped carbon quantum dots: synthesis, physicochemical properties, and their applications, *TrAC, Trends Anal. Chem.*, 2018, **103**, 87–101.

29 Y. S. Alqahtani, A. M. Mahmoud and M. M. El-Wekil, Bifunctional nanoprobe for dual-mode detection based on blue emissive iron and nitrogen co-doped carbon dots as a peroxidase-mimic platform, *Talanta*, 2023, **253**, 124024.

30 M. Vázquez-González, W. C. Liao, R. M. Cazelles, S. Wang, X. Yu, V. Gutkin and I. Willner, Mimicking horseradish peroxidase functions using Cu^{2+}-modified carbon nitride nanoparticles or Cu^{2+}-modified carbon dots as heterogeneous catalysts, *ACS Nano*, 2017, **11**, 3247–3253.

31 J. Lu, J. X. Yang, J. Wang, A. Lim, S. Wang and K. P. Loh, One-pot synthesis of fluorescent carbon nanoribbons, nanoparticles, and graphene by the exfoliation of graphite in ionic liquids, *ACS Nano*, 2009, **3**, 2367–2375.

32 H. R. H. Ali, A. I. Hassan, Y. F. Hassan and M. M. El-Wekil, Colorimetric and fluorometric nanoprobe for selective and sensitive recognition of hazardous colorant indigo carmine in beverages based on ion pairing with nitrogen doped carbon dots, *Food Chem.*, 2021, **349**, 129160.

33 R. Ali, H. Elfadilb, N. Sirag, A. S. Albalawi, A. albalawi, S. Alharbi, A. Al-anzi, S. alatawi, Y. Alhuaiti, F. T. Alsubaie, N. Aldwsari and M. M. El-Wekil, A novel red emissive glutathione-capped carbon dots embedded within molecularly-imprinted polymers for adsorption and fluorescent sensing of malachite green in food samples, *Microchem. J.*, 2025, **212**, 113376.

34 R. Dai and Y. Hu, Green/red dual emissive carbon dots for ratiometric fluorescence detection of acid red 18 in food, *Sens. Actuators, B*, 2022, **370**, 132420.

35 X. Lian, Y. Wang, Y. Huang, T. Wong and H. Sun, Self-trapped Exciton Emission from Carbon Dots investigated by Polarization Anisotropy of Photoluminescence and Photoexcitaion, *Nanoscale*, 2017, **9**, 12637–12646.

36 A. Z. Alanazi, K. Alhazzani, H. Ibrahim, A. M. Mostafa, J. Barker, A. M. Mahmoud, M. M. El-Wekil and A. B. H. Ali, pH-Sensitive blue and red N-CDs for L-asparaginase quantification in complex biological matrices, *Spectrochim. Acta, Part A*, 2025, **325**, 125161.

37 P. Liu and E. J. M. Hensen, Highly efficient and robust Au/$MgCuCr_2O_4$ catalyst for gas-phase oxidation of ethanol to acetaldehyde, *J. Am. Chem. Soc.*, 2013, **135**, 14032–14035.

38 A. M. Mahmoud, S. S. Abu-Alrub, A. O. Alqarni, M. M. El-Wekil and A. B. H. Ali, Convenient electrochemical and fluorometric dual-mode estimation of diosmin using carbon dots doped with nitrogen derived from chicken feet biowaste, *Microchem. J.*, 2023, **191**, 108929.

39 A. M. Mahmoud, M. H. Mahnashi, S. A. Alkahtani and M. M. El-Wekil, Nitrogen and sulfur co-doped graphene quantum dots/nanocellulose nanohybrid for electrochemical sensing of anti-schizophrenic drug olanzapine in pharmaceuticals and human biological fluids, *Int. J. Biol. Macromol.*, 2020, **165**(Part B), 2030–2037.

40 A. M. Mahmoud, M. M. El-Wekil, R. Ali, H. A. Batakoushy and R. Y. Shahin, Double-signal quantification of amoxicillin based on interaction with 4-aminoantipyrine at copper and nitrogen co-doped carbon quantum dots as an artificial nanozyme, *Microchem. Acta*, 2022, **189**, 183.

41 S. Huang, L. Wang, C. Huang, J. Xie, W. Su, J. Sheng and Q. Xiao, A carbon dots based fluorescent probe for selective and sensitive detection of hemoglobin, *Sens. Actuators, B*, 2015, **221**, 1215–1222.

42 A. M. Mahmoud, A. O. Alqarni, R. Ali and M. M. El-Wekil, Polyvinylpyrrolidone and 4-mercaptobenzoic acid-functionalized nickel nanoclusters for selective and sensitive detection of glutathione assisted by Fe^{3+}, *Anal. Methods*, 2025, **17**, 360–367.

43 S. T. Alsharif, A. M. Mahmoud, M. M. El-Wekil and A. B. H. Ali, Dual-signal ratiometric fluorescence detection of cholesterol using a CYS@Zn/CDs/cholesterol oxidase system, *Microchem. J.*, 2025, **208**, 112618.

44 Y. Wanga, T. Lib, L. Linb, D. Wangb and L. Feng, Copper-doped cherry blossom carbon dots with peroxidase-like activity for antibacterial applications, *RSC Adv.*, 2024, **14**, 27873–27882.

45 J. Du, S. Qi, T. Fan, Y. Yang, C. Wang, Q. Shu, S. Zhuo and C. Zhu, Nitrogen and copper-doped carbon quantum dots with intrinsic peroxidase-like activity for double-signal detection of phenol, *Analyst*, 2021, **146**, 4280–4289.

46 W. Yang, J. Fei, W. Xu, H. Jiang, M. Sakran, J. Hong, W. Zhu and X. Zhou, A biosensor based on the biomimetic oxidase Fe_3O_4@MnO_2 for colorimetric determination of uric acid, *Colloids Surf., B*, 2022, **212**, 112347.

47 J. Chen, X. Wang, Y. Wang, Y. Zhang, Z. Peng, X. Tang, Y. Hu and P. Qiu, Colorimetric detection of uric acid based on enhanced catalytic activity of cobalt-copper bimetallic-modified molybdenum disulfide, *Microchem. J.*, 2023, **189**, 108541.

48 P. Zhang, X. Wu, H. Xue, Y. Wang, X. Luo and L. Wang, Wearable transdermal colorimetric microneedle patch for Uric acid monitoring based on peroxidase-like polypyrrole nanoparticles, *Anal. Chim. Acta*, 2022, **1212**, 339911.

49 S. Ibrahim, J. Iqbal, M. Shah, W. Sun, M. Asad, M. Ullah, N. Khan, R. Ullah, Z. Iqbal, A. Badshah and U. Nishan, From Waste to Sensor: Facile Synthesis of a Copper-Doped Hydroxyapatite Nanocomposite as a Colorimetric Sensing Platform for Uric Acid, *ChemistrySelect*, 2024, e202402879.

50 Y. Wei, J. Lu, Y. Xu, X. Song, Y. Yu, H. Zhang and X. Luo, Nanozyme-immobilized cellulose membranes designed by a simple hydrogen bond-dominated for colorimetric detection of hydrogen peroxide and uric acid, *Microchem. J.*, 2023, **193**, 109113.

51 F. Li, J. Rui, Z. Yan, P. Qiu and X. Tang, A highly sensitive dual-read assay using nitrogen-doped carbon dots for the quantitation of uric acid in human serum and urine samples, *Microchim. Acta*, 2021, **188**, 311.

52 W. Hou, W. Zhao, S. Yi, W. Gao, J. Zhang, J. Zhao and X. Liu, A new application of papain: As a peroxidase-like catalyst for fluorometric detection of uric acid, *Enzyme Microb. Technol.*, 2023, **164**, 110192.

53 W. Zhang, Y. Wu, X. Liu, Y. Liu, Y. Zhang, W. Wang, X. Mu, R. Su, Y. Sun, D. Song and X. Wang, A universal sensing platform based on iron and nitrogen co-doped carbon dots for detecting hydrogen peroxide and related metabolites in human fluid by ratiometric fluorometry and colorimetry, *Spectrochim. Acta, Part A*, 2022, **272**, 121003.

54 Y. Xiao, N. Huang, J. Wen, D. Yang, H. Chen, Y. Long and H. Zheng, Detecting uric acid base on the dual inner filter effect using BSA@Au nanoclusters as both peroxidase mimics and fluorescent reporters, *Spectrochim. Acta, Part A*, 2023, **293**, 122504.

55 L. Gao, J. Zhuang, L. Nie, J. Zhang, Y. Zhang, N. Gu, T. Wang, J. Feng, D. Yang, S. Perrett and X. Yan, Intrinsic peroxidase-like activity of ferromagnetic nanoparticles, *Nat. Nanotechnol.*, 2007, **2**, 577–583.

56 Y. Guo, L. Deng, J. Li, S. Guo, E. Wang and S. Dong, Hemin-graphene hybrid nanosheets with intrinsic peroxidase-like activity for label-free colorimetric detection of single-nucleotide polymorphism, *ACS Nano*, 2011, **5**, 1282–1290.

57 W. Dong, G. Chen, L. Zhang, H. Cao, W. Shi, H. Lan and H. Zhou, Biomimetic iron-imidazole sites into metal organic framework nanoflowers as high-affinity peroxidase mimic for colorimetric biosensing, *Microchem. J.*, 2022, **175**, 107064.

58 Q. Ding, G. Y. Ren, G. Wang, M. J. Lu, J. Liu, K. Li and Y. Q. Lin, V2O5 nanobelts mimick tandem enzymes to achieve nonenzymatic online monitoring of glucose in living rat brain, *Anal. Chem.*, 2020, **92**, 4583–4591.

59 L. H. Ai, L. L. Li, C. H. Zhang, J. Fu and J. Jiang, MIL-53(Fe): a metal-organic framework with intrinsic peroxidase-like catalytic activity for colorimetric biosensing, *Chem.–Eur. J.*, 2013, **19**, 15105–15108.

60 Y. L. Liu, X. J. Zhao, X. X. Yang and Y. F. Li, A nanosized metal–organic framework of Fe-MIL-88NH_2 as a novel peroxidase mimic used for colorimetric detection of glucose, *Analyst*, 2013, **138**(16), 4526.

61 Y. Zhang, Z. Zhou, Z. F. Zhou, F. F. Wen, J. Tan, T. Peng, B. Q. Luo, H. G. Wang and S. X. Yin, A flower-like MoS_2-decorated $MgFe_2O_4$ nanocomposite: mimicking peroxidase and colorimetric detection of H_2O_2 and glucose, *Sens. Actuators, B*, 2018, **275**, 155–162.

62 L. Su, Z. Zhang and Y. Xiong, Water dispersed two-dimensional ultrathin Fe(III)-modified covalent triazine framework nanosheets: peroxidase like activity and colorimetric biosensing applications, *Nanoscale*, 2018, **10**, 20120–20125.

63 P. Das, P. Borthakur, P. K. Boruah and M. R. Das, Peroxidase mimic activity of Au–Ag/l-Cys-rGO nanozyme toward detection of Cr(VI) ion in water: role of 3,3′,5,5′-Tetramethylbenzidine Adsorption, *J. Chem. Eng. Data*, 2019, **64**, 4977–4990.

64 M. N. Ivanova, E. D. Grayfer, E. E. Plotnikova, L. S. Kibis, G. Darabdhara, P. K. Boruah, M. Das and V. E. Fedorov, Pt-decorated boron nitride nanosheets as artificial nanozyme for detection of dopamine, *ACS Appl. Mater. Interfaces*, 2019, **11**, 22102–22112.

65 Z. Xue, L. Xiong, H. Rao, X. Liu and X. Lu, A naked-eye liquid-phase colorimetric assay of simultaneous detect cysteine and lysine, *Dyes Pigm.*, 2019, **160**, 151–158.

66 J. Zhong, Y. Zhang, C. Yan, J. Chen, X. Tang, P. Xu and P. Qiu, Rapid aqueous preparation of carbon quantum dots and their application as nanozyme for the detection of hydrogen peroxide and uric acid, *Microchem. J.*, 2024, **201**, 110529.

67 R. Cheng, Z. Xiao, X. Tang, P. Xu and P. Qiu, Nickel-doped cuprous oxide nanocauliflowers with specific peroxidase-like activity for sensitive detection of hydrogen peroxide and uric acid, *Colloids Surf., B*, 2025, **245**, 114347.